

Taylor & Francis
Taylor & Francis Group

Corrosion Engineering, Science and Technology

The International Journal of Corrosion Processes and Corrosion Control

ISSN: (Print) (Online) Journal homepage: https://www.tandfonline.com/loi/ycst20

Comparative study of two equivalent circuit models for electrochemical impedance spectroscopy analysis of epoxy zinc-rich coatings

De-Ming Xie, Tian-Yu Wang, Jing-Ping Xie, Fang-Yuan Cao & Yu-Guang Wang

To cite this article: De-Ming Xie, Tian-Yu Wang, Jing-Ping Xie, Fang-Yuan Cao & Yu-Guang Wang (2023): Comparative study of two equivalent circuit models for electrochemical impedance spectroscopy analysis of epoxy zinc-rich coatings, Corrosion Engineering, Science and Technology, DOI: 10.1080/1478422X.2023.2250960

To link to this article: https://doi.org/10.1080/1478422X.2023.2250960

View supplementary material

Published online: 11 Sep 2023.

Submit your article to this journal

View related articles

View Crossmark data

Full Terms & Conditions of access and use can be found at
https://www.tandfonline.com/action/journalInformation?journalCode=ycst20

CORROSION ENGINEERING, SCIENCE AND TECHNOLOGY
https://doi.org/10.1080/1478422X.2023.2250960

I·M3 Institute of Materials, Minerals & Mining
Taylor & Francis Taylor & Francis Group

Check for updates

Comparative study of two equivalent circuit models for electrochemical impedance spectroscopy analysis of epoxy zinc-rich coatings

De-Ming Xie [a,b], Tian-Yu Wang[a], Jing-Ping Xie[c], Fang-Yuan Cao[d] and Yu-Guang Wang[e]

[a]College of Materials Science and Engineering, Zhejiang University of Technology, Hangzhou, People's Republic of China; [b]Zhejiang Juneng Co., Ltd., Tongxiang, People's Republic of China; [c]Research Institute of Petroleum Exploration and Production, SINOPEC Henan Oilfield Company, Nanyang, People's Republic of China; [d]College of International Education, Henan Normal University, Xinxiang, People's Republic of China; [e]College of Biotechnology and Bioengineering, Zhejiang University of Technology, Hangzhou, People's Republic of China

ABSTRACT

In this paper, the impedance spectra of an epoxy zinc-rich coating (ZRC) and its free film immersed in 3.5% NaCl solution are investigated, the fitting error and model parameter trends of series and nested equivalent circuit fits are compared, and the differences in the high-frequency components of the ZRC and the epoxy coatings are analyzed. The results show that the high-frequency impedance of ZRC is the contact impedance between the zinc powders (Z_m) rather than the film impedance (Z_f). The corrosion reaction of the ZRCs is controlled by the diffusion of oxygen. For ZRCs, the series equivalent circuits are more reasonable compared to the nested equivalent circuit. Based on the series equivalent circuit, the variation law of the equivalent circuit elements (resistors, capacitors and dispersion coefficient) and the correlation of these elements with low-frequency impedance modulus ($|Z|_{0.01Hz}$) and open circuit potential (OCP) are investigated in this paper.

ARTICLE HISTORY
Received 26 May 2023
Accepted 18 August 2023

KEYWORDS
Zinc-rich coatings; electrochemical impedance spectroscopy; equivalent circuit elements; series; nesting

Introduction

Electrochemical impedance spectroscopy (EIS) has been widely used in electrochemical research. The equivalent circuit-based modelling method is a common method to analyse EIS. The prerequisite for analysis based on the equivalent circuit method is the establishment of an accurate equivalent circuit model. However, electrochemical processes usually consist of multiple parallel and continuous processes, and different phenomena with similar characteristic frequencies overlap. Therefore, the interpretation of experimental results is complicated and EIS controversies are very common and span all areas of electrochemical research. For example, (1) Dominguez-Benetton et al. [1] pointed out that most studies applying EIS for microbial electrochemical systems have focused on simplifications or erroneous application of the technique. Song et al. [2] pointed out that most of the models are not convincing in explaining the EIS behaviours of mortar, cement paste, and concrete. (2) The impedance spectrum of commercial lithium-ion batteries is notoriously difficult to interpret. Churikov et al. [3] studied the electrical diffusion properties of chromium-substituted lithium-manganese spinel $Li_xMn_{1.95}Cr_{0.05}O_4$ used as cathode material for lithium-ion batteries and discussed the selection of equivalent circuits and the correct interpretation of equivalent circuit elements. (3) Hirose et al. [4] emphasised the importance of choosing a suitable equivalent circuit to model the impedance response. The search for a suitable equivalent circuit has been a goal of the chalcogenide community for the past few years.

Wang [5] pointed out that defective equivalent circuit models are often found in research papers due to the inherent deficiencies of the analytical process itself, such as the lack of rigour and standardisation of the equivalent circuit analysis method. This defect is particularly evident in the study of ZRC impedance spectra, despite the relative simplicity of the ZRC impedance spectra. There are usually two types of equivalent circuits for the ZRC impedance spectra: (1) the nested equivalent circuit (Figure 1), which is also the usual equivalent circuit for shielding coatings [6–9]. Most scholars use this equivalent circuit. (2) Series equivalent circuits (Figure 2). Figure 2(a) was first proposed by Zhang [10]. Influenced by Zhang, some Chinese scholars adopted Figure 2(a) [11,12], while scholars from other countries seldom adopted Figure 2(a). When the impedance spectrum has three arcs and the low-frequency arc corresponds to diffusion, the equivalent circuit is shown in Figure 2(b). Capacitor C behaves as a constant phase angle element (CPE). The deformation of the capacitance is due to the porous nature of the electrode. The deviation from the ideal RC is due to surface inhomogeneities and roughness effects; the nature and composition of the surface coating can be considered as a dispersion equation for the corresponding transfer function. In this paper, P_c, P_m, and P_{dl} are the dispersion coefficients of CPE_c, CPE_m, and CPE_{dl}, where CPE_c, CPE_m and CPE_{dl} are CPEs corresponding to the coating capacitance, the capacitance of the zinc powder oxidised layer, and the double layer capacitance, respectively. Z_m is usually not included in the nested equivalent circuit. Whether using both series and nested circuits, the vast majority of scholars consider the high-frequency impedance to be Z_f while the low-frequency impedance is Z_{corr}. A few believe that the high-frequency time constant corresponds to Z_{corr}, while the diffusion of O_2 occurs in the low-frequency band [13,14]. In addition, there are some other views. For example, Molnar et al. [15] suggested that the high-frequency impedance is Z_f while the low-frequency the

CONTACT Yu-Guang Wang yuguangw@zjut.edu.cn Zhejiang University of Technology, Hangzhou, Zhejiang 310014, People's Republic of China
Supplemental data for this article can be accessed online at https://doi.org/10.1080/1478422X.2023.2250960.
© 2023 Institute of Materials, Minerals and Mining Published by Taylor & Francis on behalf of the Institute

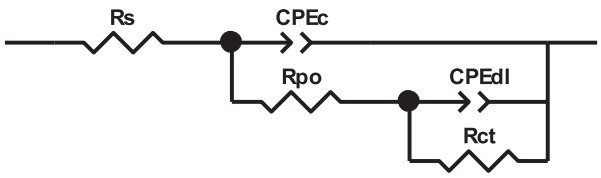


Figure 1. Mainstream equivalent circuit describing the behaviour of zinc-rich coatings. R_s, R_{po}, and R_{ct} are the solution resistance, coating pore resistance, and charge transfer resistance, respectively. Z_m is usually not included in the nested equivalent circuit.

diffusion impedance (Z_W). Xia et al. [16] suggested that the high-frequency impedance is the zinc powder corrosion impedance (Z_{corr}) and the low-frequency impedance is the corrosion reaction impedance of iron. When Z_W is present, it is controversial whether Z_W is attributed to the diffusion of O_2 or Zn^{2+}. In addition, Pereira et al. [14] noted additional arcs induced by inorganic zinc-rich layers of corrosion products but did not investigate further. Despite the great efforts of scholars, however, unfortunately, neither the connection of equivalent circuits nor the physical significance of circuit elements of the ZRC impedance spectrum have been reported in detail so far.

Common means of correctly selecting an equivalent circuit are:

(1) Consider the location of circuit components and the relationship between voltage and current distribution

The placement of circuit components and the relationship between voltage and current distribution is the first step in circuit design. Xie et al. [17] discussed the connection of basic circuit elements based on these two factors. Li et al. [18] obtained a reasonable equivalent circuit from the flow path of the disturbance current of the closed loop with defective coating.

(2) Select the equivalent circuit with high fitting accuracy
(3) Reasonableness of the changing trend of model parameters

This rationality includes the rationality of the model parameters over time and operating conditions. For example, Darowicki et al. [19] pointed out that to determine a suitable

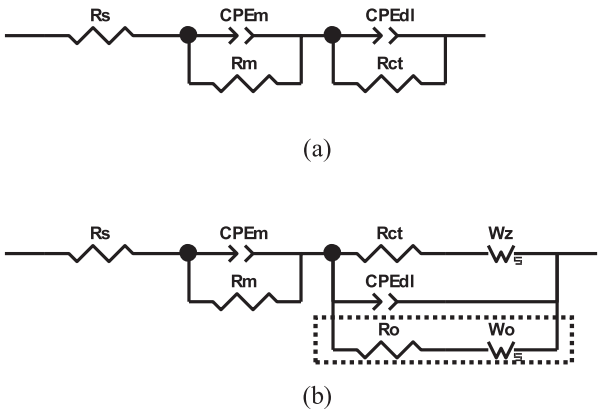


Figure 2. Series equivalent circuit with Z_m. R_m and R_O are the resistance of the zinc powder oxide layer and the oxygen reduction resistance respectively. W_Z and W_O are the diffusion elements of Zn^{2+} and O_2, respectively. The vast majority of scholars believe that the high-frequency impedance is Z_f. Labelling R_O and W_O with dashed boxes means that this part is not usually reflected. (a) Equivalent circuit of two arcs. (b) Three-arc equivalent circuit with Z_W.

equivalent model, a comprehensive analysis of equivalent circuit parameter changes during fuel cell operation is required. Song et al. [2] proposed an equivalent circuit model for the EIS of concrete, which can better explain the experimental phenomena observed by other researchers, such as the appearance of the capacitive loops in the high-frequency range, the influences of hydration time, water/cement ratio, silica fume on the loops, etc. Giner-Sanz et al. [20] performed a two-step selection process. In the first step, 4 circuit sets were preselected from the initial list of 12 circuits using the general fitting indicators. In the second step, one of the four preselected circuits was chosen based on the consistency of the fitted parameter values with the physical meaning of each parameter.

(4) EIS combined with other technologies

Nobili et al. [21] obtained simultaneously both in situ X-ray and impedance spectra of lithium desertion from $LiCoO_2$ using a specially designed electrochemical cell. The impedance spectra-dispersion was correlated with the cell parameters obtained from the X-ray energy spectrum.

Previous work by Xie et al. [22] was done on ZRCs using a series equivalent circuit containing Z_m. Based on the previous results, the group intends to prove the correctness of the series equivalent circuits containing Z_m through a more extensive and in-depth discussion. To the best of our knowledge, this is the first paper that systematically investigates the accuracy of the equivalent circuits of ZRC impedance spectra, including the electrochemical significance of the components and the way they are linked. The experimental techniques and analytical methods used in this paper are of great benefit to EIS analysis in many fields such as batteries, ceramics, and coatings.

Experimental

Mild steel specimens were sandpapered to white metal and degreased. Epoxy-polyamide zinc-rich paint (containing 78 wt-% zinc) was applied over mild steel. The ZRC free film is obtained by applying zinc-rich paint on a weighing paper. Both ZRC and its free film thickness are 60 μm, respectively. The electrochemical measurements on the coated mild steel were made using a three-electrode cell in which the sample was placed horizontally. A Perspex cylinder was fixed on the sample and filled with solution. The exposed area was 13.1 cm^2. A graphite counter electrode and a saturated calomel electrode (SCE) completed the arrangement. The EIS test apparatus of the free film is made of two thin Plexiglas tubes connected to two large Plexiglas tubes. One large Plexiglas tube is equipped with a graphite electrode connected to the research electrode of the EIS test apparatus, the other large Plexiglas tube is equipped with a graphite electrode and an SCE connected to the auxiliary electrode and the reference electrode of the EIS test apparatus, respectively. The free film is sandwiched between the two thin Plexiglas tubes. The detection contact surface is an O-ring and the test area of the free film is 4.16 cm^2. Figure 3 shows a schematic of the EIS setup for testing free film. The impedance measurements were made using an EG&G model 273 potentiostat and a model 5210 lock-in amplifier. A sine wave of 20 mV was applied across the cell. Impedance data were collected over a frequency

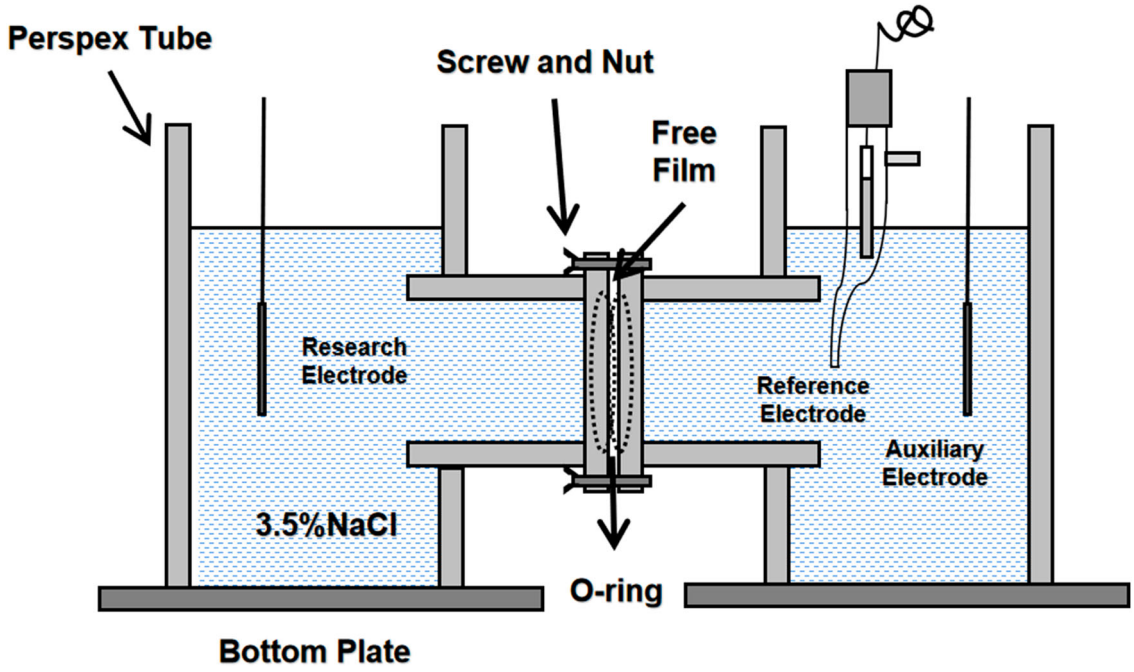


Figure 3. Schematic diagram of EIS test setup for free film.

range from 3 mHz to 120 kHz. All measurements were made in 3.5 wt-% NaCl solution at ambient temperature.

Theoretical analysis of the rationality of series equivalent circuits

Previous work demonstrated that Z_m plays a major role in high frequencies [22]. In a ZRC, the zinc powder particles can be seen as one in series together, and then the current is drawn out by the collector fluid, the steel plate. R_m and CPE_m are different properties of the same film body (zinc powder oxide layer), and if they are connected as R_{po} and CPE_c in Figure 1, the principle of electrical neutrality is violated because one end of the same film body is connected to two points of different potentials, respectively. After all, the endpoints of the same element have different potentials [23]. Therefore, if the impedance spectrum has two-time constants, the ZRC equivalent circuit can be expressed in Figure 2(a).

The qualitative models for an ideal nonporous ZRC with the molecular-diffusion transfer mechanism (B) were given in Figure 5b in the literature [24] together with the most probable equivalent circuits. This transport mechanism is closer to (B) because the corrosive medium, especially O_2, is absorbed layer by layer during the transport of the corrosive medium through the ZRCs to the steel surface. Therefore, the equivalent circuit of the ZRCs can be expressed in Figure 2(a).

In terms of structure, a ZRC can be divided into four parts: iron surface layer, inner layer, outer layer and corrosion product layer (Figure 4). The iron surface layer may be regarded as part of the inner layer. The iron surface layer is heavily corroded and dissolved by OH^- in the cathodic protection phase, thus often producing a large number of defects. The inner layer of zinc powder has good electrical conductivity with the iron substrate and corrodes quickly, which can play a cathodic protection role. The outer layer of zinc powder is mainly self-corrosion. The corrosion of the outer layer of zinc powder is mainly self-corrosion. The corrosion products OH^- and Zn^{2+} migrate partly to the surface to form a corrosion product layer and partly to the electrolyte. Because of the high Cl^- content and rapid mass transfer in the electrolyte, a large portion of OH^- and Zn^{2+} is involved in the formation of the corrosion product layer. Due to the high specific gravity of zinc powder, a very thin polymer layer is formed on the surface of the coating after curing, while in the outer layer of the coating, the percentage of a polymer is higher than that of the inner layer. However, due to the formation of corrosion product layers and the increasing proportion of self-corrosion of the surface zinc powder, the surface polymer is destroyed by the corrosion product layer and zinc powder expansion. The destruction of the surface polymer and the formation of defects in the iron surface layer cause Z_f to lose its basis of existence. In addition, the corrosion products that fill the internal pores of the coating are limited, so the internal porosity of the coating is reduced to a limited extent, if at all, due to the initial high porosity of the coating. In other words, the formation of corrosion product layers is easier than the reduction of coating porosity. The presence of corrosion product layers has become common knowledge in the field of ZRCs. In summary, the series structure of the equivalent circuit of the ZRCs is more reasonable compared to nesting in terms of the layered structure.

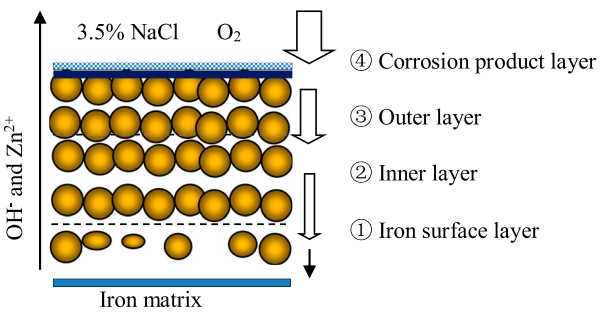


Figure 4. The layered structure of a zinc-rich coating after immersion for a period of time.

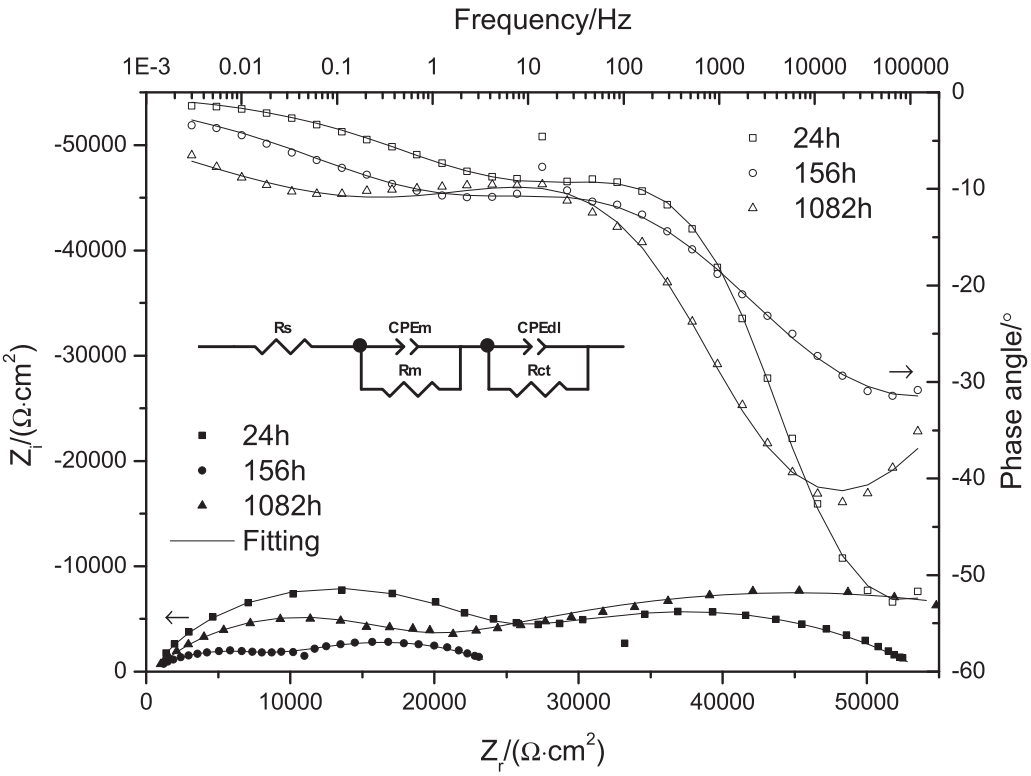


Figure 5. Nyquist curves and phase angle-frequency curves of zinc-rich free films immersed for 24, 156 and 1082 h. Scatter – experimental data, solid line – fitting results.

Impedance spectra of the zinc-rich coating and its free film

Nyquist and phase angle-time plots of the free film immersed for 24, 156, and 1082 h are given in Figure 5. Nyquist and phase angle-time plots for coatings immersed at 24, 162, 362, 1560, and 478 h, and 1704, 1918 and 1992 h are given in Figures 6–8, respectively. Modulus-time plots of the free film immersed for 24, 156, and 1082 h and the coating immersed for 24, 162, 362, and 1560 h are given in Figure 9. As can be seen from Figures 5–9, a significant difference between the free film and coating impedance spectra is that the free film impedance spectrum has always two arcs that are more clearly separated and close in size, while the low-frequency arc of the coating impedance spectrum is significantly larger than the high-frequency arc, and the two arcs are not separated. The free film impedance spectrum changed little throughout the immersing process, while the coating impedance spectra changed much more. In addition, the coating impedance spectrum appeared three arcs in the middle (478 h) and late (1704, 1918, 1992 h) of immersing.

The $|Z|_{0.01Hz}$-time curves for the ZRC and its free film and the potential-time curves for the ZRC are given in Figure 10. It can be seen from Figure 10 that the $|Z|_{0.01Hz}$ of both the free film and the coating shows a V-shaped variation. At the beginning of immersion, the increased electrolyte content in the epoxy matrix and the activation of zinc particles lead to a decrease in the impedance of both the matrix and the zinc powder oxide layer, resulting in a decrease in $|Z|_{0.01Hz}$. As the corrosion reaction proceeds, the surface area of zinc metal decreases while the corrosion product layer on the surface of zinc powder thickens, which leads to an increase in $|Z|_{0.01Hz}$. The $|Z|_{0.01Hz}$ of the last three time points of the free film decreased again, which may be because the free film was not supported and the free film structure was damaged by external stresses as well as the expansion of zinc powder after a long period of immersion. The minimum values of $|Z|_{0.01Hz}$ for the free film and the coating occur at 156 and 162 h, respectively. The Nyquist and Bode plots for the free film and the coating at 156 and 162 h, respectively, are given in Figure 11. As can be seen in Figure 11, there are large differences in the shapes of the Nyquist and Bode plots for the free film and the coating, but the dividing line between the high-frequency arc and the low-frequency arc is the same for both, i.e. about 14 Hz. The impedance modulus of the coating is significantly smaller than that of the free film in the high-frequency band. As the frequency decreases, the impedance modulus of the coating increases faster than that of the free film, exceeding that of the free film by about 0.01 Hz. This is because the high-frequency time constant corresponds to Z_m, and the zinc powder in the coating is easily activated, so the high-frequency impedance of the coating is low. The low-frequency time constant corresponds to the zinc powder corrosion, because of the difficulty of oxygen diffusion in the coating, therefore the low-frequency impedance of the coating is higher. From the OCP curve in Figure 10, after the coating is immersed into the salt solution, the OCP changes gradually from an initial potential value of $-0.949V_{SCE}$ to more positive values reaching a common level that lies intermediate between zinc and steel corrosion potentials in seawater, and approached the corrosion potential of iron after 1992 h, when the OCP = −0.634 V. A widely applicable empirical criterion for steel cathodic protection is to ensure a minimal negative value of $-0.78\ V_{SCE}$. At 1194 h, the OCP starts to become higher than −0.78 V, indicating that the coating loses cathodic protection at this point.

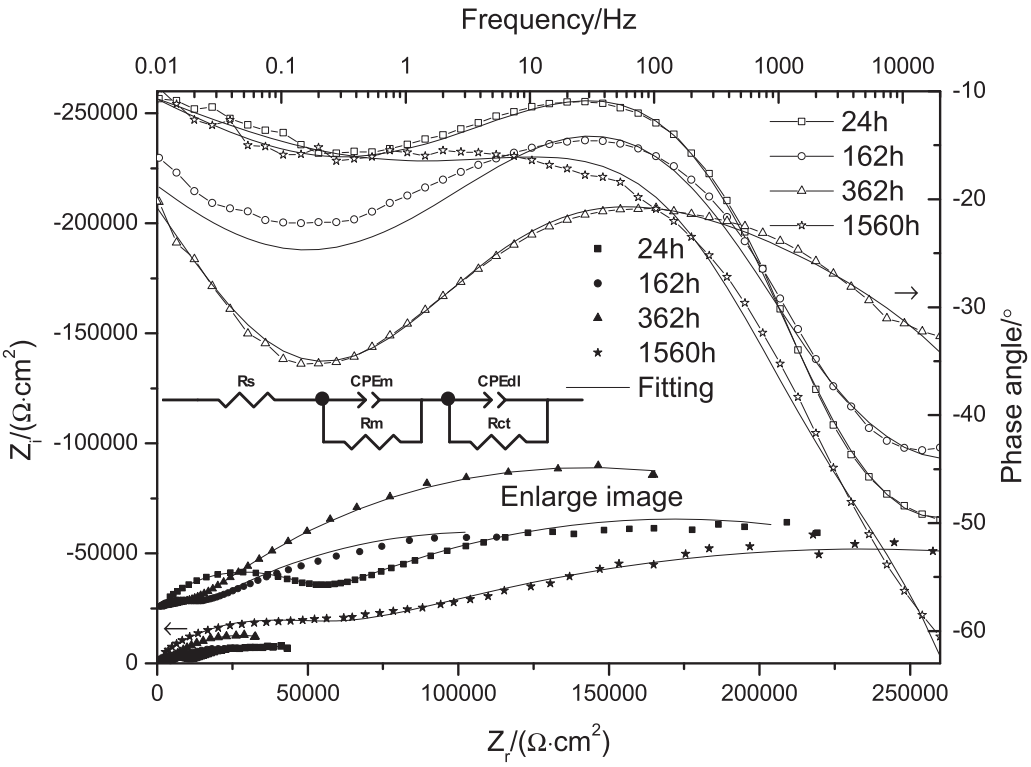


Figure 6. Nyquist curves and phase angle-frequency curves of zinc-rich coating immersed for 24, 162, 362 and 1560 h. Scatter – experimental data, solid line – fitting results.

The reasons for the difference in impedance spectra between the free film and the coating come from matrix effects; including (1) the free film is permeable while one side of the coating is blocked by the steel plate. (2) The corrosion of zinc powder in the free film is self-corrosive while in the case of the coating it includes sacrificial corrosion and self-corrosion. (3) Oxygen diffusion is much faster in free films than in coatings. Morcillo et al. [25] pointed out that if the zinc powder particles are in electrical contact with the steel, the zinc powder particles are only the site of the anodic reaction of the corrosion process, while the cathodic reaction occurs on the steel surface. Zn^{2+} and OH^{-} and Cl^{-}

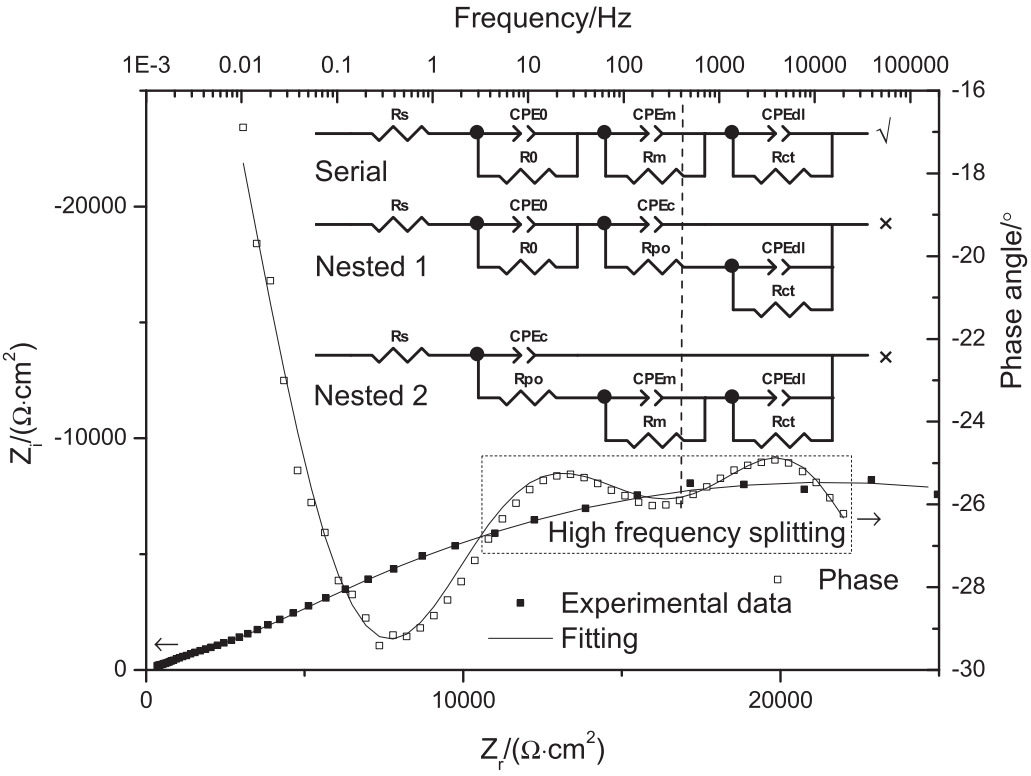


Figure 7. Nyquist curve and phase angle-frequency curve of zinc-rich coating immersed for 478 h. CPE_0, R_0 and P_0 are the capacitance, resistance, and dispersion coefficients of the corrosion product layer on the outer surface of the coating, respectively. Scatter – experimental data, solid line – fitting results.

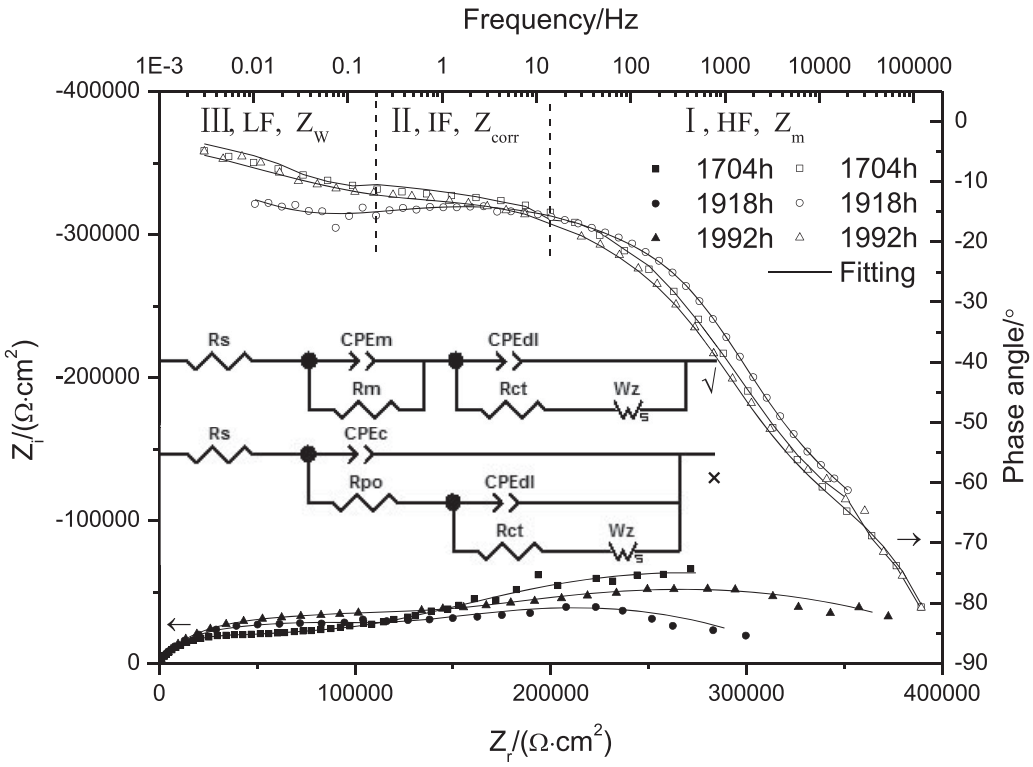


Figure 8. Nyquist and phase angle-time plots for ZRCs immersed at 1704, 1918, and 1992 h. The series circuit can be fitted better, while the nested circuit cannot fit the impedance spectra of 1918 and 1992 h (not shown in the figure). HF, IF and LF are high frequency, intermediate frequency, and low frequency, respectively.

meet in the pores of the coating away from the zinc powder particles to generate secondary corrosion products. If there is no electrical contact between the zinc powder particles and the steel, the cathodic and anodic reactions will take place on the same surface of the isolated zinc powder particles. Xie et al. [26] further developed Morcillo's theory to explain the relationship between primary corrosion product transport and secondary corrosion product species. The diffusion of Zn^{2+} and OH^- generated by sacrificial corrosion is long-range diffusion, which easily fills the coating pores and diffuses into the electrolyte. The diffusion of Zn^{2+} and OH^- generated by self-corrosion is short-range diffusion, which does not easily fill the coating pores and diffuse into the electrolyte but tends to thicken the oxide layer. In the early stage of immersion, the zinc powder corrosion products diffuse into the electrolyte and the thickening of zinc

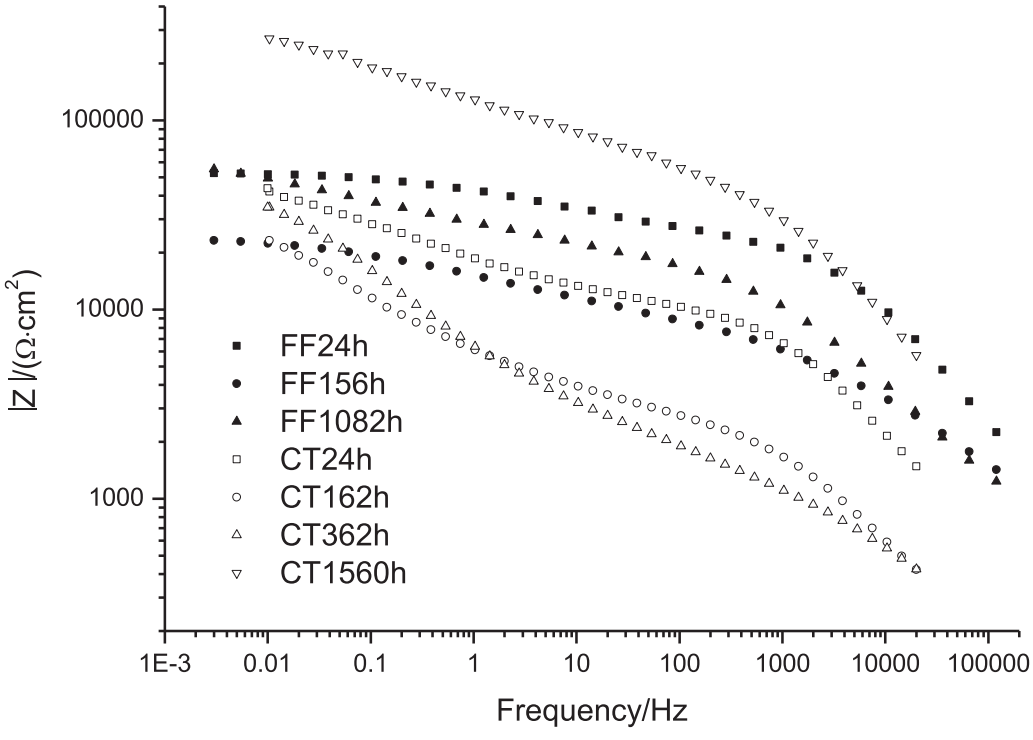


Figure 9. Modulus-frequency plots of zinc-rich free film immersed for 24, 156, 1082 h and zinc-rich coating immersed for 24, 162, 362, 1560 h. FF – Free film; CT – Coating.

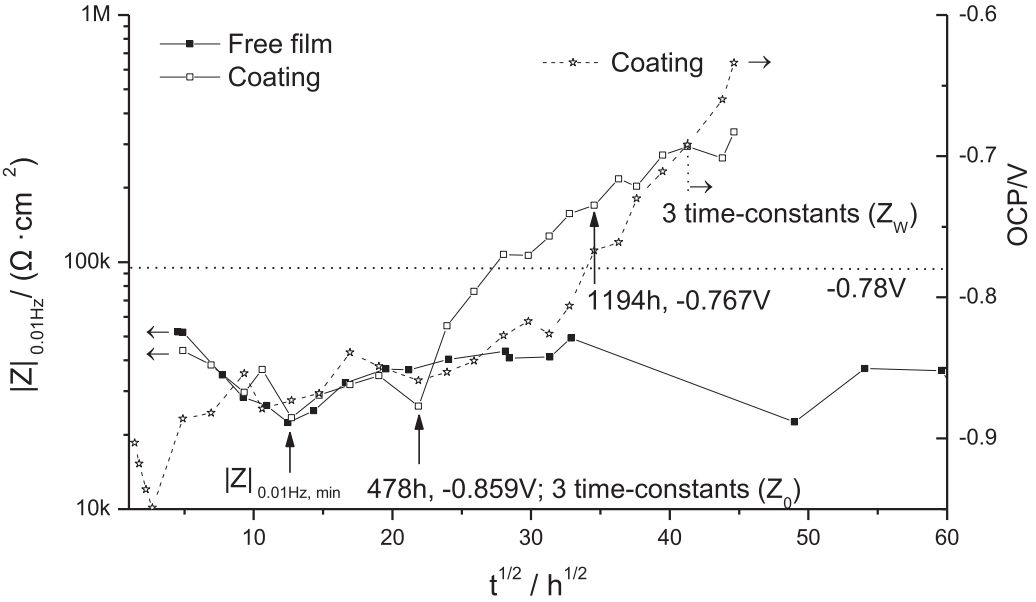


Figure 10. The $|Z|_{0.01Hz}$-time curves for the ZRC and its free film and the potential-time curves for the ZRC. The minimum values of $|Z|_{0.01Hz}$ for the free film and the coating occur at 156 and 162 h, respectively.

powder particles is not obvious, so the coating impedance is close to the free film impedance. When the ZRC potential is higher than −0.78 V, the cathodic protection of ZRCs disappears and the zinc powder becomes significantly thicker because of self-corrosion. The oxygen diffusion rate in the coating is significantly slower than that of the free film, so the impedance of the coating is significantly greater than that of the free film.

The effect of series and nested fitting of free film impedance spectra were not significantly different from the proximity of the test and fitting points, while the effect of nested fitting of coating impedance spectra was significantly worse than that of the series fitting. There are three main points:

(1) Poor nested fitting of impedance spectra for 287, 362, 573 and 670 h (Figure 12 and Table 1).
(2) A 3-time constants appear at 1704, 1918, and 1992 h when the potential is higher than the protection potential of −0.78 V. Conventional thinking considers the emergence of new arcs at low frequencies associated with diffusion (Figure 8) [27]. A series circuit with a three-time constant including the diffusion element can fit well, while the nested circuit cannot fit the impedance spectra of 1918 and 1992 h.
(3) The impedance spectrum of the ZRC at 478 h immersion showed 3-time constants (Figure 7). The new high-frequency the impedance of the corrosion product layer on the outer surface of the coating (Z_0). At this point, the OCP = −0.859 V and $|Z|_{0.01Hz} = 26\,100\ \Omega{\cdot}cm^2$. The nested circuit was poorly fitted. Cubides et al. [28] have fitted Z_0 for the first time, but only the resistance values but not the capacitance and dispersion factor values are given. The emerging high-frequency impedance is not Z_f for four reasons: (1) Comparing 478 h with its before-and-after data, it can be found that the high-frequency arc and the mid-frequency arc of 478 h are split from the high-frequency arc of the impedance spectrum at the time before and after it. A possible explanation is that near 478 h, the zinc powder reacts fast and generates a thicker layer of corrosion products, while Z_0 shows up due to the low Z_m. (2) The formation of the corrosion product layer is easier than the reduction of coating porosity. (3) The rapid disappearance of Z_f is difficult to explain. Since the coating remains cathodic protection for a considerable time thereafter, corrosion products can continue to fill the coating pores. The rapid loss of Z_0 can however be explained. Because although the coating is in the cathodic protection period, the potential has become more positive, the electrical conductivity of the outer zinc powder and the steel substrate as well as the electrical conductivity between the zinc powders decreases substantially, and the outer zinc powder enters into the self-corrosion stage before the inner zinc powder. Due to the expansion of the zinc powder, the denseness of the corrosion product layer is destroyed, and at the same time, Z_m increases leading to Z_0 cannot be presented. (4) The impedance spectra of 362, 478, and 573 h were fitted with series and nested fits, respectively, as shown in Table 2. For the impedance spectrum at 478 h, the fit results obtained from the nested1 considering Z_0 were significantly unreasonable (R_0 (11 121 $\Omega{\cdot}cm^2$) was significantly larger than R_1 (377.4 $\Omega{\cdot}cm^2$); P_1 (0.90358) and C_{dl} (0.00011), significantly higher than those of the nearby time points). The C_0 obtained for nested 2 considering Z_f is 2.637×10^{-6} F cm^{-2}, while the C_c of the 30 μm thickness epoxy-aliphatic amine coating is less than 1.593×10^{-10} F cm^{-2} within 625 h [29]. There is a difference of nearly four orders of magnitude between these two values. In addition, the P_0 was 0.53765, which was significantly smaller than 1.

Parameter evolutions of equivalent circuit elements of the impedance spectra of zinc-rich coating and its free film

The component parameters R_m and C_m, R_{ct} and C_{dl}, and P_m and P_{dl} obtained using series circuits fit are given in Figure 13, and Supplementary Figure 1 gives these

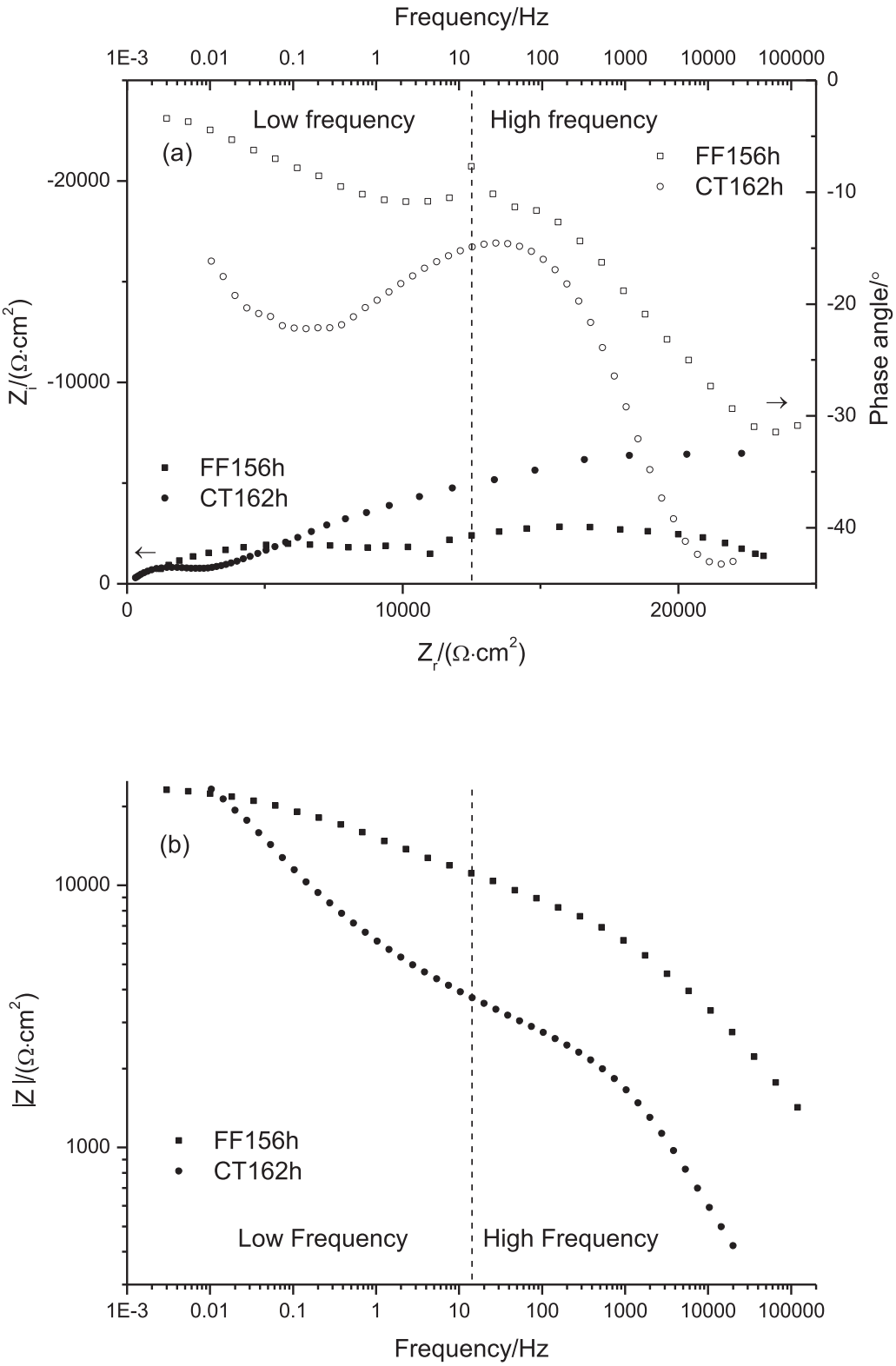


Figure 11. Nyquist and Bode plots of free film and coating at 156 and 162 h of immersion, respectively. The minimum values of $|Z|_{0.01Hz}$ for the free film and coating appear at 156 and 162 h, respectively.

component parameters obtained by fitting with both series and nested circuits. As can be seen in Supplementary Figure 1, these component parameters obtained by fitting using the two types of equivalent circuits are closer for both free films and coatings. The closeness of each parameter obtained from the fitting of the two types of equivalent circuits is greater in the early stage of immersion than in the middle and late stages of immersion. This may be because the effect of Z_f is greater at the early stage of immersion than at the middle and late stages of immersion. In the middle and late stages of immersion, the epoxy matrix gradually fails and its effect is substantially diminished.

The variation patterns of R_m, R_{ct} (decreasing and then increasing, V-shaped variation) and C_m, C_{dl} (increasing and then decreasing, inverted V-shaped variation) of the free film and the coating indicate (Figure 13(a)) that the first- and second-time constants of the impedance spectrum reflect the nature of zinc powder. The variation pattern of the resistive element is consistent with that of $|Z|_{0.01Hz}$ (comparison of Figure 13(a) and Figure 10). The variation of R_m, C_m,

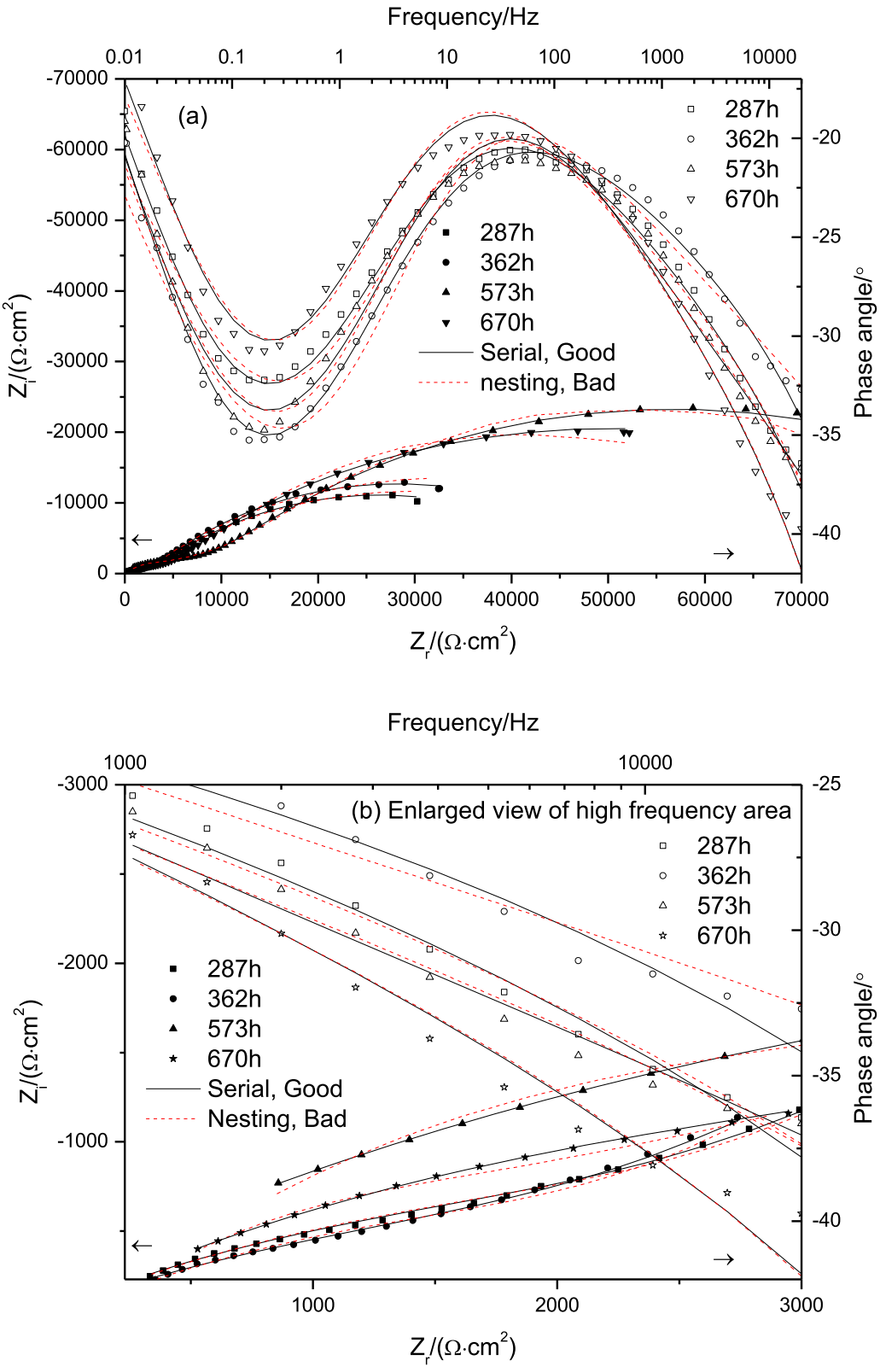


Figure 12. Nyquist plots and phase angle-frequency plots of zinc-rich coatings immersed for 287, 362, 573 and 670 h. The scatter points are the experimental data and the connecting lines are the fitted data. Scatter – experimental data, solid and dashed lines – fitting results.

R_{ct}, and C_{dl} of the coating is more significant than that of the free film, which is consistent with the variation pattern of $|Z|_{0.01Hz}$ for both in Figure 10. The decrease in R_m and the increase in C_m at the beginning of the immersion are due to the decrease in Z_f and Z_m due to the electrolyte penetration. For the coating, there is also an additional activation of OH^- leading to the thinning of the ZnO layer. The increase of R_m in the later stages of immersion is due to the thickening of the corrosion product layer on the zinc powder surface due to self-corrosion and the reduction of the effective surface area of zinc metal. The laws of change of C_m and R_{ct}, C_{dl} are not repeated.

Within 900 h, there are $R_{m,CT} < R_{m,FF}$ and $C_{m,CT} > C_{m,FF}$ (Figure 13(a)). Together with the good electrical conductivity of the steel sheet will result in $R_{ct,CT} < R_{ct,FF}$. However, the real situation is just the opposite. This is because both sides of the free film can transport oxygen and the convection in the free film is stronger than in the coating. Therefore,

Table 1. Chi-square values of series and nested equivalent circuits for zinc-rich coating immersed for 287, 362, 573, and 670 h, respectively, as well as the fitting errors of the corresponding equivalent circuit elements.

	Error, %							
	287 h		362 h		573 h		670 h	
Element	Series	Nested	Series	Nested	Series	Nested	Series	Nested
R_s	11.2	24.804	11.518	75.125	11.386	28.838	13.485	19.421
C_1	6.7648	14.291	6.9965	19.034	7.2142	15.391	8.4364	12.944
P_1	2.3477	4.2002	2.7642	5.5362	2.5809	4.5866	2.6556	3.6882
R_1	4.0801	7.9682	4.7388	10.309	4.604	8.8736	4.3382	6.1274
C_{dl}	0.9653	6.1093	0.96827	9.1741	1.2337	7.3712	1.4036	3.3997
P_{dl}	1.0688	2.5872	0.87326	3.3167	1.1362	3.0935	1.592	2.3381
R_{ct}	2.0905	3.4951	1.6422	5.9045	2.0407	4.6663	2.7981	2.7581
$\chi^2 \times 10^4$	2.2087	4.4957	1.8226	6.8985	3.3188	7.7491	5.2994	7.0966

Note: C_1 is C_c or C_m. R_1 is R_{po} or R_m. P_1 is the dispersion coefficient of CPE_1.

$R_{ct,CT} < R_{ct,FF}$. $C_{dl,CT} > C_{dl,FF}$ is because the thickness of the corrosion product layer on the surface of zinc powder in the free film is significantly greater than that of zinc powder in the coating.

In impedance spectroscopy studies of ZRCs, dispersion coefficients are usually not given. The few papers [30–32] that give dispersion coefficients also basically do not analyse them. There are two reasons for this: the factors affecting the dispersion coefficient are not clear, and the dispersion coefficient is poorly regularised. The following is a detailed analysis of the dispersion coefficient (Figure 13(c)), which hopefully can throw light on the problem.

(1) In the early and late stages of immersion, $P_{dl} < P_m$

The main factors affecting the P_m are the surface uniformity and thickness of the zinc powder oxide layer. The more uneven the surface, the smaller the P_m. The greater the thickness, the smaller the effect of roughness. Therefore the greater the thickness, the greater the P_m. The factors affecting P_{dl} include the uniformity of zinc powder corrosion, the conductivity of coating, and the thickness and surface uniformity of the zinc powder oxide layer. The more uneven the zinc powder corrosion, the worse the coating conductivity and the smaller the P_{dl}. There are more factors contributing to the reduction of P_{dl} than P_m, so $P_{dl} < P_m$ in early and late immersing.

(2) $P_{m,CT} \approx P_{m,\ FF}$ and $P_{dl,CT} \approx P_{dl,FF}$ at 24 h of immersion and the later stage of immersion

The initial conditions of the zinc powder in the coating and the free film are close at 24 h of immersion. At the later stage of immersion, both zinc powders are self-corrosive, and both P_m and P_{dl} have limit values, so both of them are close to each other.

(3) P_m decreases and then increases. The change of $P_{m,CT}$ is larger than that of $P_{m,FF}$

In the early stage of immersion, the corrosion reaction on the surface of zinc powder is uneven, and the places with high activity corrode preferentially, which leads to an increase in the unevenness of the oxide layer on the surface of zinc powder, with the result that P_m decreases. In the later stages of immersion, the corrosion rate of zinc powder decreases and the uniformity of self-corrosion is higher than that of sacrificial corrosion, so the surface layer of zinc powder becomes uniform. The consequence is an increase in P_m. The uniformity of self-corrosion is higher than that of sacrificial corrosion. Therefore, the low value of $P_{m,CT}$ is smaller than that of $P_{m,FF}$. In other words, the variation of $P_{m,CT}$ is larger than that of $P_{m,FF}$.

(4) $P_{dl,FF}$ is decreasing while $P_{dl,CT}$ is increasing and then decreasing

The continuous decrease in $P_{dl,FF}$ is due to the decrease in the percentage of active zinc due to the massive corrosion of active zinc. In the early stage of immersion, the zinc powder in the coating is gradually activated, the conductivity of the zinc powder is enhanced, the percentage of active zinc increases, and the $P_{dl,CT}$ increases. Both $P_{dl,FF}$ and $P_{dl,CT}$ decreased with decreasing active zinc ratio and zinc powder conductivity in the later stages of immersion.

The high-frequency impedance of zinc-rich coating is the contact impedance

In Supplementary Figure 1, the high-frequency impedance of both the series and nested circuits is Z_m. If the high-frequency impedance is Z_f, then R_m, C_m, and P_m will be replaced by R_{po}, C_c, and P_c, respectively. The following five facts prove that the high-frequency impedance of the ZRC

Table 2. The results of fitting the impedance spectra of zinc-rich coatings with the series and nested models for 362, 478 and 573 h of immersion, respectively.

	Serial			Nested	Nested 1	Nested 2	Nested
T/h	362	478	573	362	478		573
C_0		2.17E−05			0.000117	2.64E−6	
P_0		0.34026			0.24482	0.53765	
R_0		586.8			11121	508.9	
C_1	3.78E−05	3.87E−05	1.72E−05	2.24E−05	5.66E−06	3.60E−5	1.36E−05
P_1	0.31148	0.45298	0.34428	0.37806	0.90358	0.43407	0.37614
R_1	3718	2429	6586	3474	377.4	2596	7048
C_{dl}	7.85E−05	8.27E−05	4.90E−05	4.90E−05	0.00011	8.08E−5	3.07E−05
P_{dl}	0.59437	0.51607	0.60568	0.58097	0.55423	0.51604	0.60275
R_{ct}	49 960	37 519	76 509	65 630	29 724	37 251	96 216

Note: C_1 is C_c or C_m. R_1 is R_{po} or R_m. P_1 is the dispersion coefficient of CPE_1. The units of resistance and capacitance are $\Omega \cdot cm^2$ and $F\ cm^{-2}$ respectively.

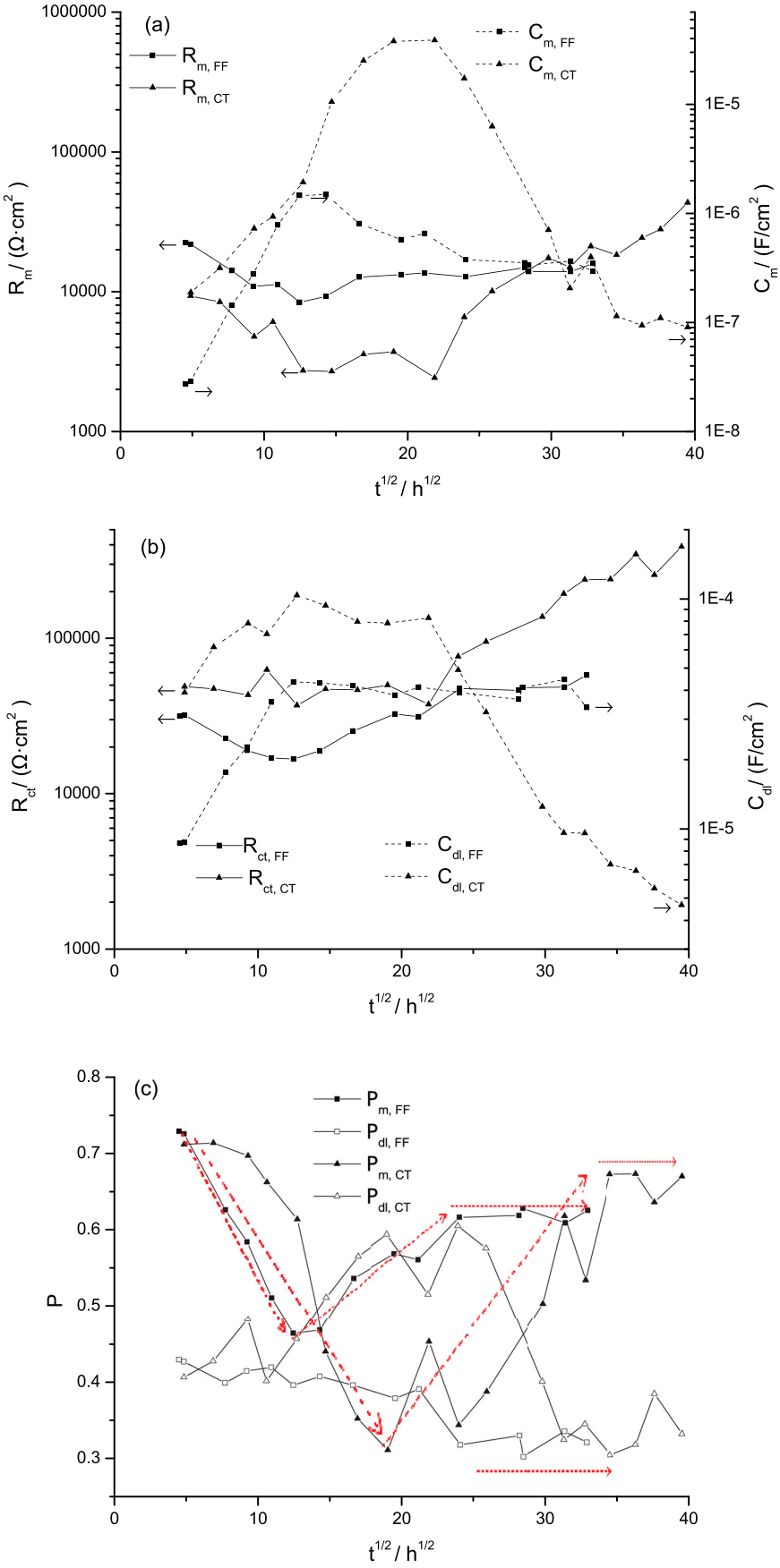


Figure 13. Component parameters R_m and C_m, R_{ct} and C_{dl}, and P_m and P_{dl} for the equivalent circuit of the EIS of zinc-rich coating and its free film obtained using series circuits fit.

and its free film is not Z_f. The comparison data were provided by Ding et al. [29]. The thicknesses of two epoxy coatings used by Ding et al. were 30 and 60 μm, respectively.

(1) The variation pattern of C_c and R_{po} of ZRC and its free film is different from that of epoxy coatings

The C_c of the ZRC and its free film showed an inverted V-shaped change, i.e. it increased first and then decreased, which was different from the stepwise increase pattern of C_c of the epoxy coatings (rapid increase in the early stage → relatively constant in the middle stage → increase in the later stage). The R_{po} of the ZRC and its free film showed a V-shaped change, i.e. it decreased first and then increased, which was different from the stepwise decrease law of the R_{po} of the epoxy coatings (rapid decrease in the early stage → relatively constant in the middle stage → decrease in the later stage).

(2) The P_c of ZRC and its free film is significantly smaller than that of epoxy coatings

The P_c of the ZRC and the free film is 0.37603–0.72786. This is much smaller than that of the epoxy coatings (close to 1).

(3) The C_c of the ZRC and its free film is much larger than that of the epoxy coatings

The C_c of the ZRC and its free film ranged from 2.46×10^{-8} to 2.24×10^{-5} F cm^{-2}, while the C_c of the 30 μm thick epoxy-aliphatic amine coating was less than 1.593×10^{-10} F cm^{-2} within 625 h. The thickness of the ZRC and its free film is 60 μm, and the thickness of the epoxy layer in it is estimated to be 24 μm, based on PVC of 60%. According to $C = \frac{\varepsilon \varepsilon_0 A}{d}$ (ε is the relative dielectric constant, ε_0 is the vacuum dielectric constant; A is the specimen area and d is the coating thickness), the capacitance of the ZRC and the free film after multiplying by 1.25 times is still much larger than that of the epoxy coatings, considering the thickness factor.

(4) The porosity of the ZRC calculated using R_{po} is several orders of magnitude lower than the true value

The porosity P can be determined by the ratio of the theoretical R_{po}^{∞} of the coating to the experimentally obtained R_{po} [29], i.e. $P = R_{po}^{\infty} / R_{po}$, where $R_{po}^{\infty} = d/k$, d is the coating thickness, k is the electrolyte conductivity, and $k = 5.5\ S \cdot m^{-1}$ for 3.5% NaCl solution (25°C). The R_{po} of the zinc-rich coating and its free film were 2918–37 536 and 9198–23 540 Ω·cm^2, respectively, so the P of the ZRC and its free film was calculated as 2.9×10^{-6}–3.74×10^{-5} and 4.63×10^{-6}–1.19×10^{-5}, respectively, which is not consistent with the high porosity of the ZRC used in this paper (usually above 1%).

(5) $R_{po,CT} < R_{po,FF}$ and $C_{c,CT} > C_{c,FF}$ within about 900 h (Supplementary Figure 1(a))

$R_{po,CT}$ should be greater than $R_{po,FF}$, and $C_{c,CT}$ should be less than $C_{c,FF}$ due to substrate effects and corrosion products filling the coating pores. If it is considered that the P of the ZRC is large and the coating rapidly saturates with water absorption, then there is $C_{c,CT} \approx C_{c,FF}$. It is easy to explain $R_{m,CT} < R_{m,FF}$ and $C_{m,CT} > C_{m,FF}$ with Z_m. This is due to the activation of the zinc powder in the coating and the thinning or small change in the thickness of the ZnO layer. On the contrary, the corrosion of zinc powder in the free film is self-corrosion, and the in-situ growth of corrosion products increases the thickness of the oxide layer on the surface of zinc powder. Thus there are $R_{po,CT} < R_{po,FF}$ and $C_{c,CT} > C_{c,FF}$.

Conclusion

Both the high-frequency and the low-frequency part of the impedance spectrum of ZRCs are associated with zinc powder. At the early stage of immersion, the high-frequency impedance is Z_m and the low-frequency impedance is Z_{corr}. The corrosion of ZRCs is controlled by the diffusion of oxygen. In the later stages of immersion, the low-frequency impedance contains information on the diffusion of Zn^{2+}. When the diffusion information is obvious, the coating impedance spectrum will include 3 arcs. ZRCs may exhibit corrosion product layer resistance while free films do not. For ZRCs, the series equivalent circuits are more reasonable compared to the nested equivalent circuit. The variation patterns of R_m, C_m, R_{ct}, and C_{dl} of ZRC and its free film are similar. The resistive element varies in a V-shape, i.e. decreases and then increases, and the capacitive element varies in an inverted V-shape, i.e. increases and then decreases. The variation pattern of the resistive element is consistent with the variation pattern of $|Z|_{0.01Hz}$.

The pattern of variation of the high-frequency component parameters of the impedance spectrum equivalent circuits for zinc-rich and epoxy coatings is very different. The P_m of the ZRCs is significantly smaller than the P_c of the epoxy coatings. The C_m of the ZRCs is much larger than the C_c of the epoxy coatings. The calculated R_{po} of ZRCs obtained using nested circuits gives a coating porosity several orders of magnitude lower than the true value. Z_f cannot explain the variation pattern of the high-frequency components of the equivalent circuit of the zinc-rich coating impedance spectrum, while Z_m can.

Disclosure statement

No potential conflict of interest was reported by the author(s).

Funding

This research was supported by the National Natural Science Foundation of China [grant numbers 51971204, 52171081], the Science Foundation of Donghai Laboratory [grant number DH-2022KF0316], the Zhejiang Provincial Natural Science Foundation of China [grant numbers LY19E010006, LY21E010005] and the Horizontal Project of Zhejiang University of Technology [grant number KYY-HX-20210359].

ORCID

De-Ming Xie http://orcid.org/0000-0002-2480-3452

References

[1] Dominguez-Benetton X, Sevda S, Vanbroekhoven K, et al. The accurate use of impedance analysis for the study of microbial

electrochemical systems. Chem Soc Rev. 2012;41(21):7228–7246. doi:10.1039/c2cs35026b
[2] Song G. Equivalent circuit model for AC electrochemical impedance spectroscopy of concrete. Cem Concr Res. 2000;30(11):1723–1730. doi:10.1016/S0008-8846(00)00400-2
[3] Churikov AV, VO R. Determination of diffusion coefficient of lithium in substituted $LiMn_{1.95}Cr_{0.05}O_4$ spinel using impedance technique. Russ J Electrochem. 2013;49(3):272–277. doi:10.1134/S1023193513030063
[4] Hirose N, West AR. Impedance spectroscopy of undoped $BaTiO_3$ ceramics. J Am Ceram Soc. 1996;79(6):1633–1641. doi:10.1111/j.1151-2916.1996.tb08775.x
[5] Wang J, Jia MY, Yang ZH, et al. On completeness of EIS equivalent circuit analysis for electrochemical corrosion process. J Chin Soc Corros Prot. 2017;37(6):479–486. Chinese.
[6] Shen L, He S, Xie W, et al. Corrosion protection of PPy-$Ti3C_2$-modifed epoxy zinc-rich coatings in dilute NaCl solution. Prog Org Coatings. 2022;172:107148. doi:10.1016/j.porgcoat.2022.107148
[7] Shen L, Li Y, Zhao W, et al. Corrosion protection of graphene-modified zinc-rich epoxy coatings in dilute NaCl solution. ACS Appl Nano Mater. 2019;2(1):180–190. doi:10.1021/acsanm.8b01821
[8] Wang S, Yang J, Cao J, et al. A mechanistic study of corrosion of graphene and low zinc-rich epoxy coatings on carbon steel in salt environment. Int J Electrochem Sci. 2019;14:9671–9681. doi:10.20964/2019.07.17
[9] Homero C, Monica G. Corrosion assessment of zinc-rich epoxy primers with carbon nanotube additions in an electrolyte with a bacteria consortium. Front Mater. 2019;6:1–12. doi:10.3389/fmats.2019.00001
[10] Zhang JQ. On EIS displays of zinc rich coatings. J Chin Soc Corros Prot. 1996;16(3):175–180. Chinese.
[11] Xie DM, Hu JM, Wang JM, et al. EIS study on zinc rich paints in 3.5% NaCl solution by double-cell test. Acta Metall Sin. 2002;15(3):299–306.
[12] Lei Y, Qiu Z, Liu J, et al. Effect of conducting polyaniline/graphene nanosheet content on the corrosion behavior of zinc-rich epoxy primers in 3.5% NaCl solution. Polymers. 2019;11:850. doi:10.3390/polym11050850
[13] Real SG, Elias AC, Vilche JR, et al. Electrochemical impedance spectroscopy study of zinc rich paints on steels in artificial sea water by a transmission line model. Electrochim Acta. 1993;38(14):2029–2035. doi:10.1016/0013-4686(93)80336-X
[14] Pereira D, Scantlebury JD, Ferreira MGS, et al. The application of electrochemical measurements to the study and behavior of zinc-rich coatings. Corros Sci. 1990;30(11):1135–1147. doi:10.1016/0010-938X(90)90061-9
[15] Molnar F, Liszi J. Protective properties of zinc-rich paints. 2001 Joint International Meeting – The 200th Meeting of the Electrochemical Society, Inc. and the 52nd Annual Meeting of the International Society of Electrochemistry; 2001 Sep 2–7; San Francisco (CA); 581.
[16] Xia W, Chen Z, Zhang G, et al. Comparison of cathodic protection processes of 40% zinc-rich coatings under immersion and atmospheric conditions: protection for defective areas. Electrochim Acta. 2021;385:138450. doi:10.1016/j.electacta.2021.138450
[17] Xie DM, Tong SP, Cao JL. Fundamental knowledge of applied electrochemistry. Beijing: Chemical Industry Press; 2013. p. 222–224. Chinese.
[18] Li ZL, Shang XB, Huang JD, et al. Electric circuit design in EIS for m etal corrosion system with coating defect. Corros Prot. 2013;34(1):52–55. Chinese.
[19] Darowicki K, Gawel L. Impedance measurement and selection of electrochemical equivalent circuit of a working pem fuel cell cathode. Electrocatalysis. 2017;8:235–244. doi:10.1007/s12678-017-0363-0
[20] Giner-Sanz JJ, Ortega EM, Pérez-Herranz V. Mechanistic equivalent circuit modelling of a commercial polymer electrolyte membrane fuel cell. J Power Sources. 2018;379:328–337. doi:10.1016/j.jpowsour.2018.01.066
[21] Nobili F, Dsoke S, Minicucci M, et al. Correlation of AC-impedance and in situ X-ray spectra of $LiCoO_2$. J Phys Chem B. 2006;110(23):11310–11313. doi:10.1021/jp0606356
[22] Xie DM, Tong SP, Feng H, et al. Influence of the pigment shape on the electrochemical behaviors of zinc-rich paint coatings in 3.5% NaCl solution. Acta Metall Sin. 2005;41(7):769–774. Chinese.
[23] Wang J. Electrochemical impedance spectroscopy equivalent circuit model of corrosion process introduction to the analysis method. Friends Corros Prot. 2016;9. https://corrdata.org.cn/dhTJDAOHANG/xinxiziyuan/kepuqikan/2016-11-01/3047.html. Chinese.
[24] Golovin VA, Dobriyan SA, Lukin VB, et al. On the choice of an equivalent circuit for the description of electrochemical impedance spectra of Zn-filled polymer primers and coatings. Prot Met Phys Chem Surf. 2017;53(7):1271–1279. doi:10.1134/S2070205117070061
[25] Morcillo M, Barajas R, Feliu S, et al. A SEM study on the galvanic protection of zinc-rich paints. J Mater Sci. 1990;25:2441–2446. doi:10.1007/BF00638039
[26] Xie DM, Huang K, Feng X, et al. Improving the performance of zinc-rich coatings using conductive pigments and silane. Corros Eng Sci Techn. 2020;55(7):539–549. doi:10.1080/1478422X.2020.1759484
[27] Abreu CM, Izquierdo M, Keddam M, et al. Electrochemical behavior of zinc-rich epoxy paints in 3% NaCl solution. Electrochim Acta. 1996;41:2405–2415. doi:10.1016/0013-4686(96)00021-7
[28] Cubides Y, Su SS, Castaneda H. Influence of zinc content and chloride concentration on the corrosion protection performance of zinc-rich epoxy coatings containing carbon nanotubes on carbon steel in simulated concrete pore environments. Corrosion. 2016;72(11):1397–1423. doi:10.5006/2104
[29] Ding R, Gui TJ, Jiang JM, et al. Electrochemical impedance spectroscopy study of corrosion behavior of solvent-free epoxy coatings on steel substrate. J Vac Sci Technol. 2017;37(2):165–176. Chinese.
[30] Meroufel A, Touzain S. EIS characterisation of new zinc-rich powder coatings. Prog Org Coat. 2007;59(3):197–205. doi:10.1016/j.porgcoat.2006.09.005
[31] Goodarzi IM, Farzam M, Shishesaz MR, et al. Eco-friendly, acrylic resin-modified potassium silicate as water-based vehicle for anticorrosive zinc-rich primers. J Appl Polym Sci. 2014;131:40370.
[32] Mirzaie GI, Farzam M, Shishesaz MR, et al. Effect of molar ratio and resin modification on the protection properties of zinc-rich alkali silicate primer. Iran J Oil Gas Sci Techn. 2014;3(1):41–53.